

A SIX YEAR IMAGE-SUBTRACTION LIGHT CURVE OF SN 2010JL

E. O. OFEK¹, B. ZACKAY², A. GAL-YAM¹, J. SOLLERMAN³, C. FRANSSON³, C. FREMLING⁴, S. R. KULKARNI⁴,
P. E. NUGENT^{5,6}, O. YARON¹, M. M. KASLIWAL⁴, F. MASCI⁷, R. LAHER⁷

Draft of March 7, 2019

ABSTRACT

SN 2010jl was a luminous Type II_n supernova (SN), detected in radio, optical, X-ray and hard X-rays. Here we report on its six year *R*- and *g*-band light curves obtained using the Palomar Transient Factory. The light curve was generated using a pipeline based on the proper image subtraction method and we discuss the algorithm performances. As noted before, the *R*-band light curve, up to about 300 days after maximum light is well described by a power-law decline with a power-law index of $\alpha \approx -0.5$. Between day 300 and day 2300 after maximum light, it is consistent with a power-law decline, with a power-law index of about $\alpha \approx -3.4$. The longevity of the light curve suggests that the massive circum-stellar material around the progenitor was ejected on time scales of at least tens of years prior to the progenitor explosion.

Subject headings: stars: mass-loss — supernovae: general — supernovae: individual: SN 2010jl, PTF 10aaxf — techniques: photometric

1. INTRODUCTION

The emission from some supernovae (SNe) is powered by the conversion of the SN-ejecta kinetic energy into visible light over time scales of months to years (orders of magnitude shorter than in SN remnants). This mechanism is responsible for powering the light curves of at least some Type II_n SNe (e.g., Schlegel et al. 1990; Chevalier & Fransson 1994; Chugai & Danziger 1994; Ofek et al. 2013a; see Filippenko 1997; Gal-Yam 2017 for the definition of Type II_n SNe).

SN 2010jl (PTF 10aaxf) is a Type II_n SN discovered by Newton & Puckett (2010). The SN took place in a star-forming galaxy (UGC 5189A) at a distance of about 50 Mpc. Reaching a visual magnitude of approximately 13, this SN was observed across the electromagnetic spectrum (e.g., Patat et al. 2011; Smith et al. 2011; Stoll et al. 2011; Chandra et al. 2012, 2015; Zhang et al. 2012; Moriya et al. 2013; Ofek et al. 2013b, 2014a; Fransson et al. 2014; Aartsen et al. 2015; Ackermann et al. 2015; Jencson et al. 2016). The SN radiated $\gtrsim 6 \times 10^{50}$ erg (Fransson et al. 2014), likely from the conversion of the kinetic energy in the ejecta to visible light via interaction of the ejecta with circumstellar material (CSM) around the SN progenitor. Visible light and X-ray observations contain evidence that the CSM is likely very massive (e.g., Zhang et al. 2012; Chandra et

al. 2012, 2015; Fransson et al. 2014; Ofek et al. 2014a) with order-of-magnitude mass-estimates in the range of 5–15 M_{\odot} . *NuSTAR* hard X-ray observations of this system can be used to estimate the shock velocity, which was found to be consistent with the estimates based on the visible light data (Ofek et al. 2014a), and with the spectroscopic estimates (Borish et al. 2015).

Recently, Fox et al. (2017) presented late time *HST* observations that constrain the progenitor luminosity. Dwek et al. (2017) use this, as well as *Spitzer* observations, to constrain the dust mass around the progenitor. They argue that if the progenitor is assumed to be similar to η Car, then about 4 magnitudes of extinction are required, which suggests $\gtrsim 10^{-3} M_{\odot}$ of dust around the progenitor, prior to its explosion. Gall et al. (2014) argue, based on an extinction derived from the supernova line ratios, that at late times (868 days) about $2 \times 10^{-3} M_{\odot}$ were formed around SN 2010jl (assuming dust is mainly composed of Carbon, but could be up to an order of magnitude larger for silicates). This estimate assumes that the conditions at the line-formation site do not vary with time. Sarangi et al. (2018) estimated a dust mass of order $10^{-2} M_{\odot}$ (at an age of few hundreds days after explosion). Sarangi et al. (2018) estimated a dust mass of 2×10^{-3} – $10^{-2} M_{\odot}$, depending on dust composition, at day 844 after the explosion.

Given the long timescales over which SN 2010jl is visible, this object presents a unique opportunity to study the physics of collisionless shocks propagating within massive CSM (e.g., Katz et al. 2011; Murase et al. 2011, 2014). Here we present a six year light curve of SN 2010jl. We measure the SN light curve using the proper image subtraction algorithm of Zackay, Ofek, & Gal-Yam (2016; ZOGY), and we evaluate the performance of this method in a complex environment.

In §2 we present the SN observations. In §3 we describe our image subtraction photometry pipeline, while in §4 we discuss its performances, and we conclude in §5.

2. OBSERVATIONS AND LIGHT CURVE

¹ Benozio Center for Astrophysics and the Helen Kimmel center for planetary science, Weizmann Institute of Science, 76100 Rehovot, Israel.

² School of Natural Sciences, Institute for Advanced Study, 1 Einstein Drive, Princeton, New Jersey 08540, USA

³ Department of Astronomy, The Oskar Klein Centre, Stockholm University, AlbaNova University Centre, SE-106 91 Stockholm, Sweden

⁴ Cahill Center for Astronomy and Astrophysics, California Institute of Technology, Pasadena, CA 91125, USA

⁵ Computational Cosmology Center, Lawrence Berkeley National Laboratory, 1 Cyclotron Road, Berkeley, CA 94720, USA

⁶ Department of Astronomy, University of California, Berkeley, CA 94720-3411, USA

⁷ Infrared Processing and Analysis Center, California Institute of Technology, Pasadena, CA 91125, USA

The Palomar Transient Factory (PTF) and its continuation project the intermediate PTF (iPTF; Law et al. 2009; Rau et al. 2009), using the 48-inch Oschin Schmidt Telescope, observed the field of SN 2010jl over 600 times. The data reduction is described in Laher et al. (2014), while the photometric system is discussed in Ofek et al. (2012a).

The SN is located on top of a bright star-forming region ($r \approx 15.5$ mag). The bright host galaxy makes its necessary to use image-subtraction based photometry. We constructed image-subtraction-based light curves in the Mould R and g bands, based on all the images in which the transient location is more than 100 pixels from a CCD edge. In total we used 485 Mould R -band images and 185 g -band images⁸. The analysis was performed using tools available in the MATLAB astronomy and astrophysics toolbox⁹ (Ofek 2014).

For the reference image, we selected all the images taken prior to 2010 May 23. This amounts to 27 R -band and 12 g -band images. The image-subtraction photometry pipeline is briefly described in §3. The photometric calibration was done against the Pan-STARRS-1 catalog (PS1; Chambers et al. 2016).

The image-subtraction-based measurements are listed in Table 1, and the entire R -band light curve is presented in Figure 1, while the g -band light curve is shown in Figure 2. The photometry in the plots are corrected for Milky-Way extinction ($E_{B-V} = 0.027$ mag; Schlegel et al. 1998; Cardelli et al. 1989).

We fit a broken power-law to the light curves. Each power law fit is of the form

$$L = L_0(t - t_0)^{-\alpha}, \quad (1)$$

where L is the luminosity, t is the time in Julian Days (JD), t_0 was set to JD= 2455474.5 (see justification in Ofek et al. 2014a), and α is the power-law index. The best-fit power-law indices are listed in Table 2.

3. IMAGE-SUBTRACTION PIPELINE

Our pipeline¹⁰ is based on the image subtraction algorithm of Zackay, Ofek, & Gal-Yam (2017; ZOGY), and it contains the following steps: Image cutouts of about 1000×1000 pix, containing the requested target, are read into memory. The images are converted to units of electrons, by multiplying the images by their gain. The background is estimated both locally on scales of 64×64 arcsec, and globally. We then apply `mextractor` to estimate the PSF for each image, extract the sources and measure their position, shapes, aperture photometry and PSF photometry (Ofek et al. in prep.).

We solve the astrometry of the images using `astrometry.m` (Ofek 2018), in respect to GAIA-DR2 reference stars (GAIA Collaboration et al. 2018), and use SWarp (Bertin 2010) to interpolate the images to the same grid. The reference image is photometrically calibrated using either SDSS (Ahn et al. 2014), PS-1 (Flewelling et al. 2016) or APASS (Henden et al. 2015) catalogs, and we also fit for relative zero points between the images (e.g., Ofek et al. 2011 Appendix A). Next,

we populate the mask image, associated with each science image, with bits indicating saturated pixels, flat-field holes¹¹, and cosmic rays. We read the observing date and exposure time from the images header and calculate the mid-exposure Julian Day (JD). A reference image is constructed either using proper coaddition or simple weighted coaddition (Zackay & Ofek 2017a,b). The astrometric noise relative to the reference image is estimated, and we perform the image subtraction, and read the PSF photometry at the target position using Equation 41 in ZOGY. Our pipeline also provide meta data information (see §4).

One difference from the ZOGY algorithm is that we propagate the astrometric errors not only into the score¹² image, but also into the relative uncertainty in the photometry. Any astrometric errors, due to e.g., scintillation noise, will effect the subtraction and hence the photometry. The error in the PSF photometry is linear with the astrometric uncertainty. Therefore, the effect of such errors on the photometry can be estimated from the image gradients. Specifically, the additional fractional error in the flux due to the astrometric uncertainty is

$$\sigma_{\text{astrom}} = \frac{\sqrt{(\sigma_x \nabla_x S_N)^2 + (\sigma_y \nabla_y S_N)^2}}{F_S}. \quad (2)$$

Here σ_x and σ_y are the astrometric uncertainties in the x and y positions, respectively, measured in pixels; ∇_x and ∇_y are the gradients in the x and y directions, respectively; S_N is given by Equation 31 in ZOGY. and F_S is the flux normalization of the image subtraction statistics (Equation 42 in ZOGY).

4. TESTING THE LIGHT CURVE

Here we present some of the sanity tests we performed on the light curve. We demonstrate that such tests are useful for identifying problems and should be used routinely.

For all the images taken in each band, we also generated light curves for 1000 random image positions. We use these light curves to calculate two properties. The first is the *epochal* χ^2 presented in Figure 3. This is the χ^2 over all 1000 random positions in one epoch, where the errors in the χ^2 are obtained using Equation 41 in Zackay et al. (2016). If the fluctuations in the background of the subtracted image in each epoch are represented by the error estimate, then this epochal χ^2 should be of the order of the number of degrees of freedom (about 1000). We note that we do not expect that the epochal χ^2 will be distributed exactly like a χ^2 distribution with the relevant number of degrees of freedom. This is because, in our ZOGY implementation we used a global background variance value, while in practice the variance is slightly position dependent. This allows us to identify epochs in which the photometry is highly uncertain. Furthermore, we use it to correct the photometric errors by a multiplicative factor of

$$\max[1, \sqrt{\chi_{\text{epochal}}^2 / \text{dof}}]. \quad (3)$$

⁸ The images were taken at two PTF fields and CCDs. PTF field 3159 and CCDID 6, and PTF field 100072 and CCDID 10.

⁹ <https://webhome.weizmann.ac.il/home/eofek/matlab/>

¹⁰ Implemented in `ImUtil.pipe.imsub.lightcurve`.

¹¹ Flat-field holes are negative features in the science image generated by leftover sources in the flat image.

¹² Denoted S in ZOGY.

TABLE 1
PTF PHOTOMETRIC MEASUREMENTS OF SN 2010JL

Band	JD-JD ₀ (day)	Mag (mag)	Mag Err. (mag)	Counts (count)	Counts error (count)	$\chi^2_{epochal}$
<i>g</i>	-563.8546	NaN	NaN	-7.56×10^3	6.73×10^3	991.0
<i>g</i>	-563.6819	NaN	NaN	8.24×10^1	3.61×10^3	674.6
<i>g</i>	-562.7827	NaN	NaN	-3.43×10^3	4.39×10^3	1141.3
<i>g</i>	-562.6970	NaN	NaN	8.08×10^2	7.73×10^3	1242.3
<i>g</i>	-557.8225	NaN	NaN	-4.10×10^3	8.99×10^3	814.9

NOTE. — Image-subtraction-based photometry of SN 2010jl. JD₀ = 2455474.5, corresponding to about 20 days prior to *I*-band maximum light (Stoll et al. 2011). The PS1-based photometric zero points, not corrected for color term, are 30.213 and 32.443, for *g* and *R* band, respectively. The magnitudes are shown in Luptitude units (Lupton, Gunn, & Szalay 1999) in order to deal with negative fluxes. Note that there is a small color term, between the PS1 and PTF magnitudes (see Ofek et al. 2012a for PTF filters transmission). Photometry is done in the PTF native photometric system (i.e., the color term was fitted, and the color of the SN was set to zero). This table is published in its entirety in the electronic edition. A portion of the full table is shown here for guidance regarding its form and content.

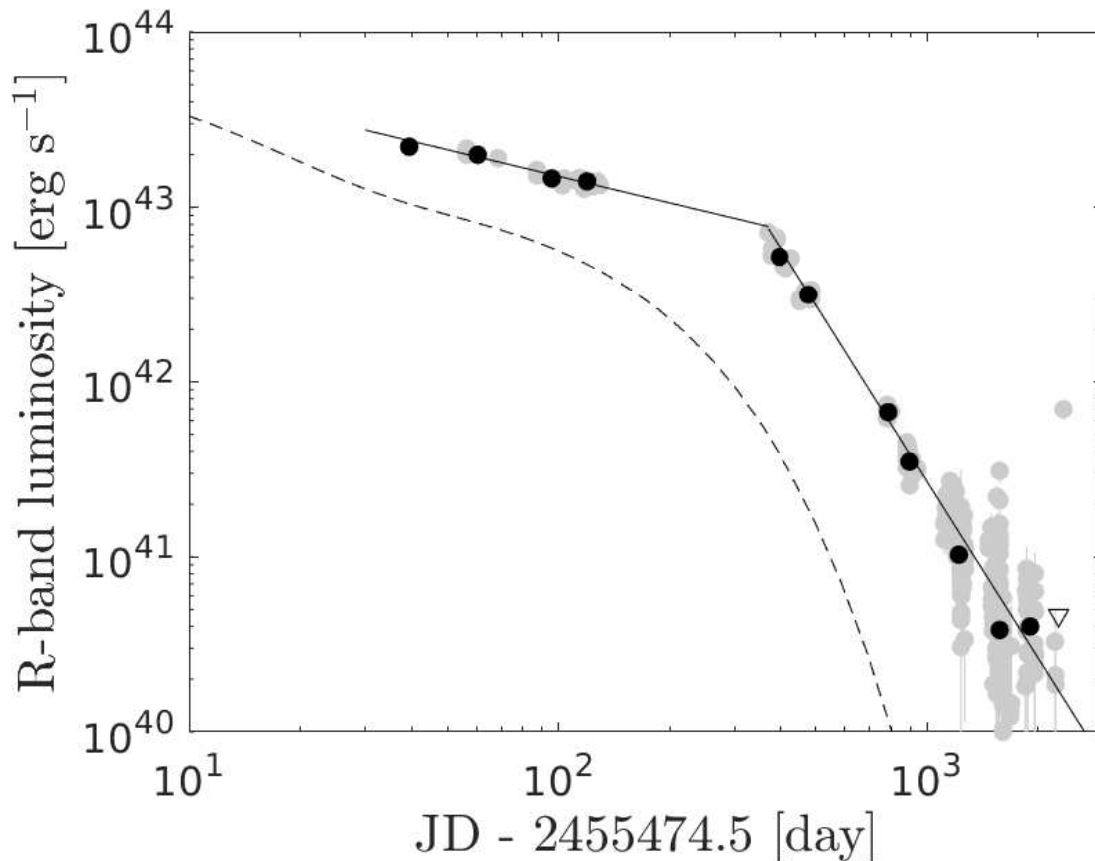


FIG. 1.— The PTF *R*-band light curve of SN 2010jl (gray circles). The black circles are binned photometry (including negative flux measurements), while the empty-black triangle represents a binned $3\text{-}\sigma$ upper limit on the luminosity. The luminosity light curve is corrected for Galactic extinction. The dashed line shows the expected radiated bolometric luminosity from one solar mass of radioactive Nickel 56.

The second property is the *positional* χ^2 (Figure 4). This is the χ^2 in each random position over all epochs. This is useful in order to identify issues related to background estimation.

Figures 3-4 identify some epochs with bad subtractions, and epochs in which our errors were underestimated. We corrected such errors using Equation 3. The underestimation of the errors is likely due to errors in the flux matching process, background subtraction, PSF estimation, and source noise due to the host galaxy

flux. We note that we propagated the photometric errors due to the astrometric uncertainty using Equation 2.

Another interesting test is to correlate the residuals from the power-law fit, when the SN is bright at the first 360 days, with various parameters. We attempted to correlate the flux residuals with parameters like the airmass, flux matching (β), the mean level of the subtraction image, the derived flux normalization (F_S ; Equation 42 in ZOGY), and the epochal χ^2 . Spearman rank correlations of the residuals from the best-fit power law with

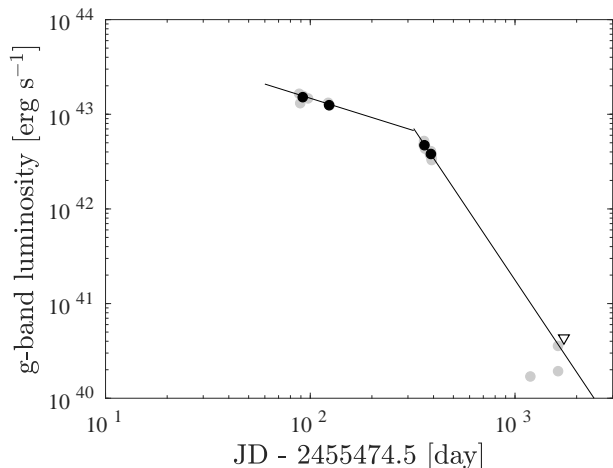


FIG. 2.— Like Figure 1, but for the g -band. The individual measurements after 1000 days are consistent with no detection.

TABLE 2
SN 2010JL POWER-LAW FIT

Band	Time range (day)	α
R	0–360	-0.50 ± 0.04
R	360–1000	-3.36 ± 0.04
g	0–360	-0.68 ± 0.1
g	360–1000	-3.2 ± 0.3

NOTE. — Power-law index fits to SN 2010jl light curve in specific time ranges and bands, relative to $JD_0 = 2455474.5$. To estimate the uncertainty on the fitted power law, the individual photometric errors were renormalized such that the χ^2 per degree of freedom will be one. Since in g band the SN is detected only for about three years after maximum light, we fit power laws only in the first 1000 days.

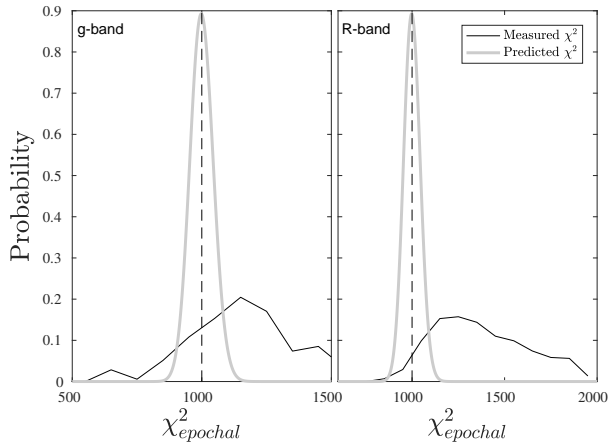


FIG. 3.— The epochal χ^2 for g band (left) and R band (right).

these parameters were consistent with zero, with false-alarm probability smaller than 10% in all cases.

5. DISCUSSION

In §5.1 we discuss the implication of the six-year light curve, the pre-explosion observations are presented in §5.2, and the implications for the pre-explosion mass loss are discussed in §5.3.

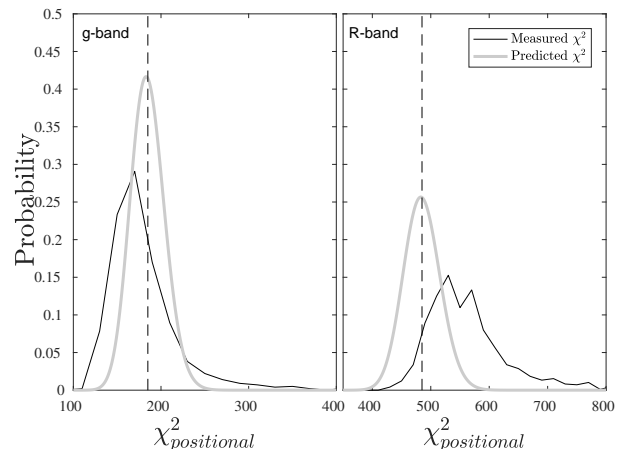


FIG. 4.— The positional χ^2 for g band (left) and R band (right).

5.1. The six-year light curve of SN 2010jl

As noted by Ofek et al. (2014a), the SN light curve is consistent with a broken power-law light curve. Figures 1–2 show the R - and g -band light curves, respectively, of SN 2010jl. The gray lines represent the best-fit broken power laws to the R -band data. The most important feature is that six years after maximum light, the SN is still detected in the R band and that the late-time ($t - JD_0 > 1000$ days) light curve follows the power law fitted in the 360–1000-day range.

In the case of SN 2010jl, a shock breakout likely occurred within the CSM – a so-called wind shock breakout (e.g., Ofek et al. 2010; Chevalier & Irwin 2011). The hydrodynamics of ejecta with a power-law velocity distribution moving into a CSM with a density profile that follows another power-law distribution is described by an analytical self-similar solution (Chevalier 1982). This hydrodynamical solution dictates the rate of kinetic energy conversion into thermal energy and radiation (e.g., Fransson 1984; Chugai & Danziger 1994; Svirski et al. 2012; Moriya et al. 2013; Ofek et al. 2014a), which is yet another power law. The light curve of SN 2010jl at early times (about one year prior to maximum light) is consistent with a power-law decay with a power-law index of $\alpha \approx -0.5$. Assuming spherical symmetry, power-law density distributions of the CSM and ejecta, negligible bolometric correction¹³, and using the Chevalier (1982) self-similar solution, the observed power-law index suggest a CSM density profile of $\approx r^{-2.2}$ to $r^{-2.3}$ for radiative/convective stars (see e.g., Ofek et al. 2014a).

We note that the exact value of the power law slope depends on t_0 and any unknown bolometric corrections (see Ofek et al. 2014a for the dependence of the power-law on t_0 and bolometric correction). There are several possible explanations for the broken power-law light curve (e.g., geometry, van Marle 2010; and variations in the density profile, Chandra et al. 2015). However, it is not clear to us what is the correct explanation for the discontinuity in the optical light curve of SN 2010jl.

5.2. Pre-explosion variability

¹³ This is consistent with the roughly constant effective temperature reported in Ofek et al. (2014a).

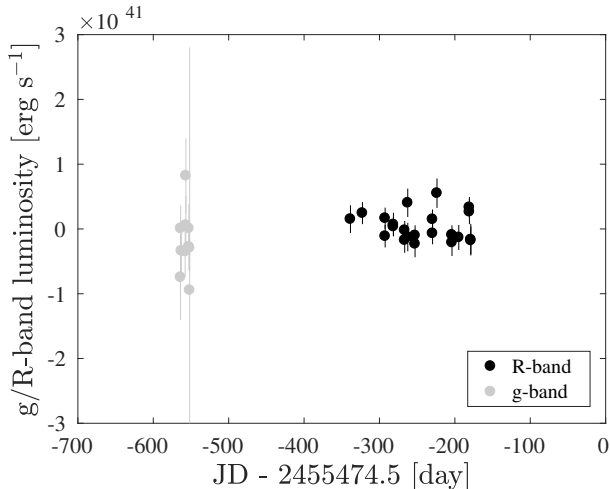


FIG. 5.— The pre-explosion R (black circles) and g -band (gray circles) light curves of SN 2010jl.

In recent years a large number of precursors – outbursts prior to the SN explosion, mainly prior to Type IIn SNe, were reported (Foley et al. 2007; Pastorello et al. 2007; Mauerhan et al. 2013; Pastorello et al. 2013; Corsi et al. 2014; Fraser et al. 2013; Ofek et al. 2013b, 2014b, 2016; Strotjohann et al. 2016; Nyholm et al. 2017; Arcavi et al. 2017). Furthermore, Ofek et al. (2014b) showed that these precursors are common in the final years prior to an explosion of a Type IIn SN. SN 2010jl was included in the sample of Ofek et al. (2014b), and no precursor was found. The amount of pre-explosion data we have for this SN is small compared with other SNe in the Ofek et al. (2014b) sample. Furthermore, it is possible that the amplitude of any variability will be attenuated by contribution from the underlying bright star-forming region or dust.

Figure 5 shows the pre-explosion light curve at the SN location. Since these observations were also used as a reference image, all we can say is that the progenitor did not show short-term variability (i.e., smaller than a few weeks). We set a $5\text{-}\sigma$ upper limit of absolute magnitude of -13.8 and -13.9 in g and R bands, respectively,

for any short term variability during these observations. These absolute magnitudes are corrected only for Galactic extinction.

5.3. Implications for pre-explosion mass-loss

The late-time light curve of SN 2010jl is still remarkably bright in comparison with any reasonable contribution from ^{56}Ni (see Fig. 1). Since, at late times (≈ 400 days), the shock ejecta velocity is of the order of $3000\text{--}5000\text{ km s}^{-1}$ (Ofek et al. 2014a), this implies that there is still a considerable density of CSM at distances of $\sim 2 \times 10^{16}$ cm from the SN. Assuming a CSM velocity of 100 km s^{-1} (Fransson et al. 2014), we conclude that the CSM was ejected of the order of

$$\sim 60 \left(\frac{v_{\text{CSM}}}{100\text{ km s}^{-1}} \right)^{-1} \text{ yr}, \quad (4)$$

prior to the SN explosion, where v_{CSM} is the CSM ejection velocity. We note, for comparison, that the age of the η Car Homunculus Nebula is estimated to be about 1800 yr (Morse et al. 2001; Smith et al. 2017), and that Sarangi et al. (2018) argued for the existence of a cavity in SN 2010jl’s CSM.

This paper is based on observations obtained with the Samuel Oschin Telescope as part of the Palomar Transient Factory project, a scientific collaboration between the California Institute of Technology, Columbia University, Las Cumbres Observatory, Oskar Klein Centre, the Lawrence Berkeley National Laboratory, the National Energy Research Scientific Computing Center, the University of Oxford, and the Weizmann Institute of Science. E.O.O. is grateful for support by grants from the Willner Family Leadership Institute Ilan Gluzman (Secaucus NJ), Israel Science Foundation, Minerva, BSF, BSF-transformative, Weizmann-UK, and the I-Core program by the Israeli Committee for Planning and Budgeting and the Israel Science Foundation (ISF). B.Z. is grateful for receiving the support of the Infosys membership fund.

REFERENCES

- Aartsen, M. G., Abraham, K., Ackermann, M., et al. 2015, *ApJ*, 811, 52
- Ackermann, M., Arcavi, I., Baldini, L., et al. 2015, *ApJ*, 807, 169
- Ahn, C. P., Alexandroff, R., Allende Prieto, C., et al. 2014, *ApJS*, 211, 17
- Arcavi, I., Howell, D. A., Kasen, D., et al. 2017, *Nature*, 551, 210
- Bertin, E. 2010, *Astrophysics Source Code Library*, ascl:1010.068
- Borish, H. J., Huang, C., Chevalier, R. A., et al. 2015, *ApJ*, 801, 7
- Cardelli, J. A., Clayton, G. C., & Mathis, J. S. 1989, *ApJ*, 345, 245
- Chambers, K. C., Magnier, E. A., Metcalfe, N., et al. 2016, arXiv:1612.05560
- Chandra, P., Chevalier, R. A., Irwin, C. M., et al. 2012, *ApJ*, 750, L2
- Chandra, P., Chevalier, R. A., Chugai, N., Fransson, C., & Soderberg, A. M. 2015, *ApJ*, 810, 32
- Chevalier, R. A. 1982, *ApJ*, 259, 302
- Chevalier, R. A., & Fransson, C. 1994, *ApJ*, 420, 268
- Chevalier, R. A., & Irwin, C. M. 2011, *ApJ*, 729, L6
- Chugai, N. N., & Danziger, I. J. 1994, *MNRAS*, 268, 173
- Corsi, A., Ofek, E. O., Gal-Yam, A., et al. 2014, *ApJ*, 782, 42
- Dwek, E., Arendt, R. G., Fox, O. D., et al. 2017, *ApJ*, 847, 91
- Filippenko, A. V. 1997, *ARA&A*, 35, 309
- Flewelling, H. A., Magnier, E. A., Chambers, K. C., et al. 2016, arXiv:1612.05243
- Foley, R. J., Smith, N., Ganeshalingam, M., et al. 2007, *ApJ*, 657, L105
- Fox, O. D., Van Dyk, S. D., Dwek, E., et al. 2017, *ApJ*, 836, 222
- Fransson, C. 1984, *A&A*, 133, 264
- Fransson, C., Ergon, M., Challis, P. J., et al. 2014, *ApJ*, 797, 118
- Fraser, M., Magee, M., Kotak, R., et al. 2013, *ApJ*, 779, L8
- Gaia Collaboration, Brown, A. G. A., Vallenari, A., et al. 2018, arXiv:1804.09365
- Gall, C., Hjorth, J., Watson, D., et al. 2014, *Nature*, 511, 326
- Gal-Yam, A. 2017, *Handbook of Supernovae*, ISBN 978-3-319-21845-8. Springer International Publishing AG, 2017, p. 195, 195
- Henden, A. A., Levine, S., Terrell, D., & Welch, D. L. 2015, *American Astronomical Society Meeting Abstracts*, 225, 336.16
- Jencson, J. E., Prieto, J. L., Kochanek, C. S., et al. 2016, *MNRAS*, 456, 2622
- Katz, B., Sapir, N., & Waxman, E. 2011, arXiv:1106.1898
- Lahe, R. R., Surace, J., Grillmair, C. J., et al. 2014, *PASP*, 126, 674
- Law, N. M., et al. 2009, *PASP*, 121, 1395
- Lupton, R. H., Gunn, J. E., & Szalay, A. S. 1999, *AJ*, 118, 1406
- Mauerhan, J. C., Smith, N., Filippenko, A. V., et al. 2013, *MNRAS*, 430, 1801
- Moriya, T. J., Maeda, K., Taddia, F., et al. 2013, *MNRAS*, 435, 1520
- Morse, J. A., Kellogg, J. R., Bally, J., et al. 2001, *ApJ*, 548, L207

- Murase, K., Thompson, T. A., Lacki, B. C., & Beacom, J. F. 2011, *Phys. Rev. D*, 84, 043003
- Murase, K., Thompson, T. A., & Ofek, E. O. 2014, *MNRAS*, 440, 2528
- Newton, J., & Puckett, T. 2010, *Central Bureau Electronic Telegrams*, 2532, 1
- Nyholm, A., Sollerman, J., Taddia, F., et al. 2017, *A&A*, 605, A6
- Ofek, E. O., Rabinak, I., Neill, J. D., et al. 2010, *ApJ*, 724, 1396
- Ofek, E. O., Frail, D. A., Breslauer, B., et al. 2011, *ApJ*, 740, 65
- Ofek, E. O., Laher, R., Law, N., et al. 2012a, *PASP*, 124, 62
- Ofek, E. O., Fox, D., Cenko, S. B., et al. 2013a, *ApJ*, 763, 42
- Ofek, E. O., Sullivan, M., Cenko, S. B., et al. 2013b, *Nature*, 494, 65
- Ofek, E. O., Zoglauer, A., Boggs, S. E., et al. 2014a, *ApJ*, 781, 42
- Ofek, E. O., Sullivan, M., Shaviv, N. J., et al. 2014b, *ApJ*, 789, 104
- Ofek, E. O. 2014, *Astrophysics Source Code Library*, 1407.005
- Ofek, E. O., Cenko, S. B., Shaviv, N. J., et al. 2016, *ApJ*, 824, 6
- Ofek, E. O. 2018, submitted
- Patat, F., Taubenberger, S., Benetti, S., Pastorello, A., & Harutyunyan, A. 2011, *A&A*, 527, L6
- Pastorello, A., Smartt, S. J., Mattila, S., et al. 2007, *Nature*, 447, 829
- Pastorello, A., Cappellaro, E., Inserra, C., et al. 2013, *ApJ*, 767, 1
- Rau, A., et al. 2009, *PASP*, 121, 1334
- Sarangi, A., Dwek, E., & Arendt, R. G. 2018, *ApJ*, 859, 66
- Schlegel, E. M. 1990, *MNRAS*, 244, 269
- Schlegel, D. J., Finkbeiner, D. P., & Davis, M. 1998, *ApJ*, 500, 525
- Smith, N., Li, W., Miller, A. A., et al. 2011, *ApJ*, 732, 63
- Smith, N. 2017, *MNRAS*, 471, 4465
- Stoll, R., Prieto, J. L., Stanek, K. Z., et al. 2011, *ApJ*, 730, 34
- Strotjohann, N. L., Ofek, E. O., Gal-Yam, A., et al. 2015, *ApJ*, 811, 117
- Svirski, G., Nakar, E., & Sari, R. 2012, arXiv:1202.3437
- van Marle, A. J., Smith, N., Owocki, S. P., & van Veelen, B. 2010, *MNRAS*, 407, 2305
- Zackay, B., Ofek, E. O., & Gal-Yam, A. 2016, *ApJ*, 830, 27
- Zackay, B., & Ofek, E. O. 2017a, *ApJ*, 836, 187
- Zackay, B., & Ofek, E. O. 2017b, *ApJ*, 836, 188
- Zhang, T., Wang, X., Wu, C., et al. 2012, *AJ*, 144, 131